nature photonics

LETTERS

PUBLISHED ONLINE: 29 MAY 2011 | DOI: 10.1038/NPHOTON.2011.102

Broadband graphene polarizer

Qiaoliang Bao[1], Han Zhang[2,5], Bing Wang[3], Zhenhua Ni[4], Candy Haley Yi Xuan Lim[1], Yu Wang[1], Ding Yuan Tang[2] and Kian Ping Loh[1]*

Conventional polarizers can be classified into three main modes of operation: sheet polarizer using anisotropic absorption media, prism polarizer by refraction and Brewster-angle polarizer by reflection[1]. These polarizing components are not easily integrated with photonic circuits. The in-line fibre polarizer, which relies on polarization-selective coupling between the evanescent field and birefringent crystal[2] or metal[3–7], is a promising alternative because of its compatibility with most fibre-optic systems. Here, we demonstrate the operation of a broadband fibre polarizer based on graphene, an ultrathin two-dimensional carbon material. The out-coupled light in the telecommunication band shows a strong *s*-polarization effect with an extinction ratio of 27 dB. Unlike polarizers made from thin metal film, a graphene polarizer can support transverse-electric-mode surface wave propagation due to its linear dispersion of Dirac electrons.

Graphene has attracted a high level of research interest because of its exceptional electronic transport properties[8], which have great potential in applications in the field of nanoelectronics. Its photonic properties are equally remarkable[9,10]. The universal optical conductance of graphene is defined by the fine structure constant and is independent of frequency over a wide range[11]. Its zero bandgap affords the benefit of high-bandwidth detection of light[12]. The facile saturation of its absorption due to Pauli blocking enables graphene to be used as a saturable absorber in broadband, ultrafast mode-locked lasers for use in telecommunications[13,14]. Its two-dimensional nature also allows the fabrication of photonic circuits with ultrathin optical elements. In these circuits, graphene may be used to carry out the creation, routing, modulation or detection of light. Light modulation by means of polarization management is vital to avoid signal fading and error in coherent optic communications as well as in optical gyroscopes and interferometric sensors. The ability to couple and modulate light with such an ultrathin guiding material has yet to be experimentally demonstrated despite several theoretical investigations[15–19].

In this Letter, we demonstrate the coupling, guiding and polarizing of electromagnetic waves by graphene. The polarization mechanism is attributed to the differential attenuation of two polarization modes. In conventional two-dimensional electron systems, for example consisting of an ultrathin metal film and a GaAs/AlGaAs quantum well, the local dynamic conductivity described by the Drude model has the form $\sigma(\omega) = in_s e^2/m(\omega + i\tau)$ (ref. 20), where n_s, e, m and τ are the concentration, charge, effective mass and scattering rate of two-dimensional electrons, respectively. As $\sigma(\omega)$ has a positive imaginary part σ'', only the transverse-magnetic (TM) mode can propagate in such structures; the transverse-electric (TE) mode is forbidden at a single interface between a metal and a dielectric according to boundary conditions[19]. The spectra of electromagnetic modes are sensitive to the electron (hole) mass. However, the situation in graphene is quite different because of its massless Dirac fermions. The dynamic conductivity of graphene can be determined from the Kubo formalism, consisting of intraband and interband contributions: $\sigma(\omega) = \sigma_{\mathrm{intra}}(\omega) + \sigma_{\mathrm{inter}}(\omega)$ (see Methods)[21,22]. The imaginary part σ'' plays an important role in the propagation of surface waves in a graphene sheet. The imaginary part of $\sigma_{\mathrm{intra}}(\omega)$ is always positive so that the TM mode can be supported (providing the chemical potential $\mu \neq 0$). At $\hbar\omega/2 > |\mu|$, the contribution of interband optical transition gives rise to the negative imaginary part of $\sigma_{\mathrm{inter}}(\omega)$, which supports the conditions for TE mode existence[19]. This TE mode has a weakly damped wave propagating along the graphene sheet at close to the velocity of light[19], and it is this that underpins the basis for the development of a broadband graphene TE-pass polarizer.

Figure 1a presents a schematic of an in-line fibre-to-graphene coupler, capable of coupling electromagnetic waves into a two-dimensional graphene plane. Optical images of the graphene optical device are shown in Fig. 1b,c. In this configuration, the dispersion and birefringence (the effective index difference) of the planar waveguide play important roles in the effective coupling of light and the selectivity for wavelength and polarization. Similar to surface plasmon polaritons (SPP) in metal films[23], radiation originating from leaky modes or surface scattering are key signatures of strong perturbations of the fundamental core mode by graphene in terms of coupling and guiding. The radiative green light (Fig. 1d) that originates from the interaction of the graphene and fibre can be observed easily with the naked eye, indicating effective coupling. Such leakage radiation shows distance-dependent damping (Supplementary Fig. S2c). With the help of a polarization analyser equipped with an optical microscope (Supplementary Fig. S2), it was found that the radiative light is highly *s*-polarized (orthogonal to the plane of incidence), which attests to coupling and guiding of the TE mode by the graphene. This polarizing effect is highly reproducible when white light is used as the excitation source (Supplementary Fig. S3), suggesting the possibility of broadband polarization of light.

The polarization extinction ratios at both visible and near-infrared (NIR) frequencies were measured (see Methods and Supplementary Information). Using visible light as the excitation source (Supplementary Fig. S4), monolayer graphene with propagation distance $L_G = 2.1$ mm gave an extinction ratio of 14.2 dB for green (532 nm) light and 13.9 dB for blue (488 nm) light, as shown in Fig. 2a. The maximum output occurred at $\theta = 0^\circ$, and the minimum appeared at $\theta = 90^\circ$, confirming the *s*-polarized nature of transmitted light. Even stronger polarization occurred for NIR wavelengths, with an extinction ratio of ~18.3 dB at 980 nm, ~15.7 dB at 1,300 nm, ~18.4 dB at 1,480 nm

[1]Department of Chemistry, National University of Singapore, 3 Science Drive 3, Singapore 117543, [2]School of Electrical and Electronic Engineering, Nanyang Technological University, Singapore 639798, [3]Institute of Materials Research and Engineering, Agency for Science, Technology and Research (A*STAR), 3 Research Link, Singapore 117602, [4]Department of Physics, Southeast University, Nanjing, China 211189, [5]Service OPERA-photonique, Université libre de Bruxelles (U.L.B.), 50 Avenue F. D. Roosevelt, CP 194/5, B-1050 Bruxelles, Belgium. *e-mail: chmlohkp@nus.edu.sg

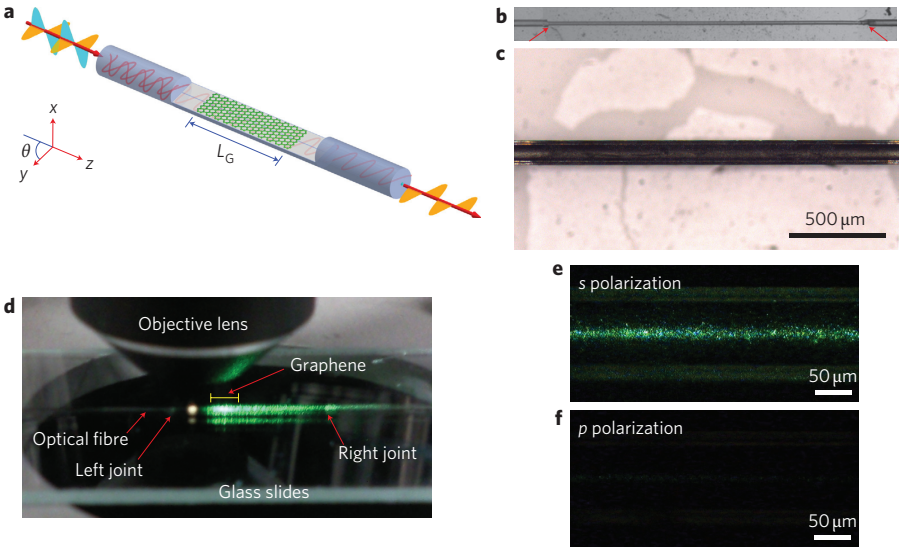

Figure 1 | Fibre-to-graphene coupler and optical polarization. a, Schematic model of fibre-to-graphene coupler based on a side-polished optical fibre. L_G, propagation distance (length of covered graphene film). Polarization angle θ is defined as the angle between the polarization direction of the analyser (in x–y plane) and the graphene plane (y–z plane). **b**, Optical image of laterally polished optical fibre. Red arrows indicate joints (separated by ~15 mm) between the side-polished and unpolished sections. **c**, Optical image showing a planar section of optical fibre covered by few-layer (~4–5 layers) graphene film, which gives a darker contrast compared to the naked region. **d**, Optical image showing radiative green light from the fibre-to-graphene coupler with excitation at 532 nm (~1 mW). **e**,**f**, Polarized optical image of the radiative light along the s (**e**) and p (**f**) polarizations (taken under the same illumination light intensity). The radiative line along the axis of the fibre core in **e** indicates a strong interaction between the graphene and the excitation light.

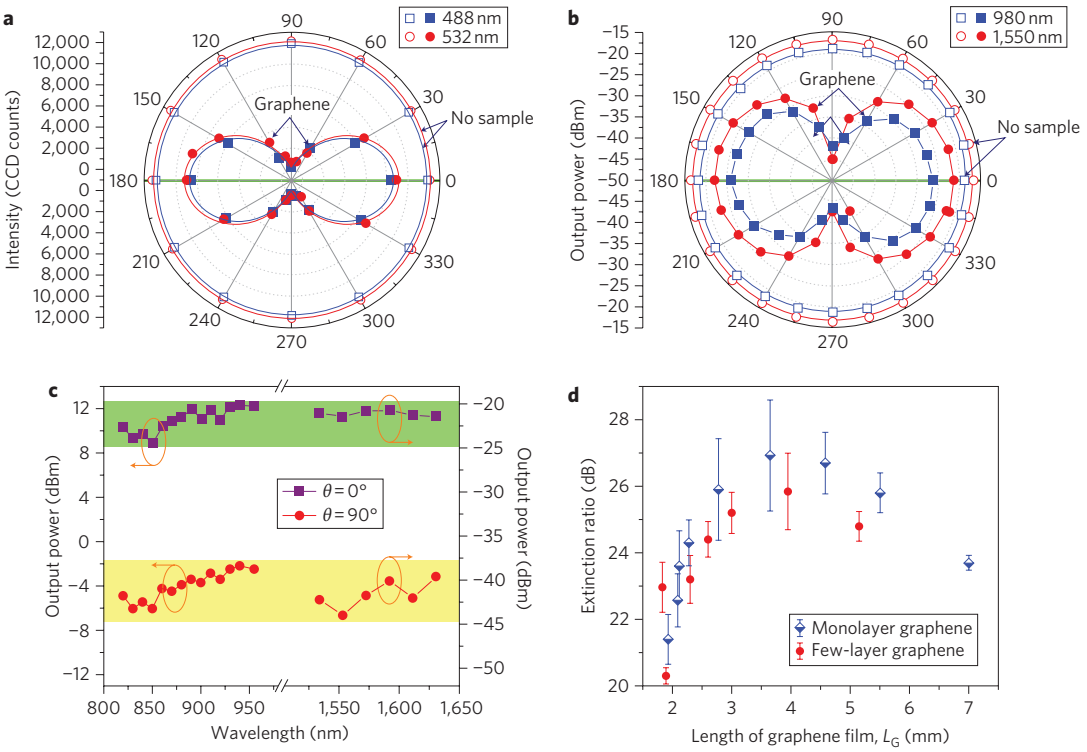

Figure 2 | Broadband polarizing effect of graphene. a, Polar image measured at 488 and 532 nm ($L_G = 2.1$ mm). The curves are $\cos^2$ fits. The green line indicates the projection of the graphene film in the x–y plane (Fig. 1a). CCD, charge-coupled device. **b**, Polar image measured at 980 nm ($L_G = 3$ mm) and 1,550 nm ($L_G = 2.1$ mm). **c**, Polarization measurements conducted in the wavelength range 820–955 nm ($L_G = 3$ mm) and in the telecommunication C-band from 1,530 to 1,630 nm ($L_G = 2.1$ mm). The output maximum (green area) and minimum (yellow area) were recorded at polarization angles $\theta = 0°$ and 90°, respectively. **d**, Polarization extinction ratio as a function of L_G measured at 1,550 nm. The saturation and reduction of the extinction ratio at larger L_G are attributed to the limitation of our measurement system because both polarization modes are greatly weakened and the TM polarization mode is attenuated beyond the detection minimum of the power meter (−50 dBm). The error bars represent standard deviation of the measurements.

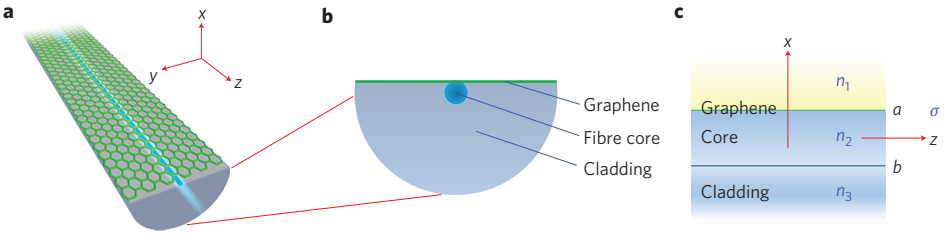

Figure 3 | Numerical model. a,**b**, Perspective view (**a**) and cross-section (**b**) of the side-polished optical fibre. **c**, Two-dimensional theoretical model showing the graphene/silica fibre and cladding/core interfaces in the plane of incidence (σ, surface conductivity of graphene; refractive index, $n_1 = 1.0$, $n_2 = 1.468$, $n_3 = 1.463$). In the model, we assume z to be the direction of propagation, x is perpendicular to the graphene plane and y is invariant.

and ~23.6 dB at 1,550 nm (Fig. 2b, Supplementary Fig. S9). When ~1 mW (0 dBm) light (1,550 nm) was directed into the fibre-to-graphene coupler, the output light at $\theta = 90^\circ$ and 270° was greatly suppressed to give -45 ± 0.3 dBm, whereas outputs at $\theta = 0^\circ$ and 180° gave a value of -21.4 ± 0.5 dBm. Polarization measurements were also carried out in continuous wavelengths in the range 820–955 nm and in the telecommunication C-band at 1,530–1,630 nm (Fig. 2c), giving extinction ratios of $\sim 15 \pm 0.6$ dB and $\sim 19 \pm 2.5$ dB, respectively. These results attest to the potential of graphene to function as a broadband polarizer. A control experiment was also conducted on the as-received side-polished optical fibre without graphene cladding, resulting in the observation of no polarizing effect. When considering the insertion loss of the measurement system (~15 dB at 1,550 nm), the insertion loss due to graphene was ~5 dB, which is higher than that reported for commercial devices, which have typical insertion losses below 1.5 dB. The insertion loss here is mostly linked to the continuity and uniformity of the graphene film (see Supplementary Information for more details).

Controlling the propagation distance in a graphene waveguide affords a route for scaling the difference between the two polarization modes. For example, increasing the lateral dimension of the graphene film will give a larger extinction ratio, as illustrated in Fig. 2d. A maximum value of ~27 dB can be obtained with $L_G \approx 3.5$ mm. The electronic structure of monolayer graphene is preserved in few-layer graphene due to the misoriented stacking order and effective decoupling of adjacent layers[8,13], so few-layer graphene gives a similar polarizing effect to that of monolayer graphene, but with a lower extinction ratio (maximum, ~25 dB) and moderate dependence on L_G. The magnitude of the extinction ratio is comparable to those of similarly configured polarizers using metal thin film (39 dB for indium[4] and 47 dB for gold[3] at 820 nm, 24 dB for silver at 1,300 nm and 31 dB for aluminium[24] at 1,550 nm). In metal-clad polarizers, broadband polarization and high extinction ratios can be achieved by engineering more complex structures incorporating resonant buffer layers[5,7], an index overlay[6] or multilayer leaky structures[25]. It should be emphasized that the selective, broadband transmittance of the TE mode in a graphene-based polarizer is simple and robust, in contrast to the situation for metal polarizers, where stringent control of the thickness of the film is necessary to fulfil the phase-matching conditions[26,27]. For comparison, when a gold thin film (thickness, 50 nm; $L_G = 3.5$ mm) was evaporated on the side-polished fibre, we only observed a TM pass polarizing effect with an extinction ratio of 5.5 dB at 980 nm and 10.4 dB at 1,550 nm (Supplementary Fig. S13).

To obtain further insight, a theoretical model was built to study the guiding of surface waves by graphene (Fig. 3). Because of the infinitesimal thickness of graphene, it can be considered as an embedded conductive interface between two dielectrics (silica core/graphene/air)[16,28]. The effective index method[29] was used to calculate the dispersion relation (see Methods and Supplementary Information). To account for the cylindrical geometry effect of the fibre core, integration was carried out along the curved boundary, assuming that the cylindrical waveguide consisted of planar counterparts with continuously varying thickness.

Multimode propagation is possible below the cutoff wavelength of single-mode fibre. In the fibre-to-graphene coupler, coupling and confinement by graphene induces higher-order leaky modes[16], which play a key role in filtering out TM polarization. Figure 4a depicts the real part of the effective index (n_{eff}) of the possible existing modes in the visible–NIR frequency range. The value of n_{eff} in the guided modes lies between n_2 and n_3 (horizontal dashed green lines), and the modes manifest as leaky waves in a certain wavelength range where $n_{eff} < n_3$. Figure 4b shows the imaginary part of n_{eff}. It correlates with propagation loss through the attenuation constant $\alpha = \mathrm{Im}(n_{eff})k_0$, as illustrated in Fig. 4c. It is apparent that the attenuation of TM polarization is always larger than that of TE polarization for all leaky modes. This means that TM modes suffer greater loss than TE modes with the same propagation distance. Because higher-order leaky modes decay very quickly and have relatively small propagation lengths (Fig. 4d), the lowest-order leaky modes dominate the loss regime in the corresponding wavelength range; that is, the first-order mode ($m = 1$) for $\lambda > 1{,}180$ nm, the second-order mode ($m = 2$) for $\lambda \in$ (687 nm, 1,180 nm), the third-order mode ($m = 3$) for $\lambda \in$ (523 nm, 687 nm) and the fourth-order mode ($m = 4$) for $\lambda \in$ (400 nm, 523 nm). Furthermore, our simulation reveals a nonzero and relatively larger magnitude for the TE modal field compared to the TM modal field at the graphene/fibre interface (Supplementary Fig. S15a). We can therefore conclude that the polarizing effect observed is a direct consequence of the difference in the attenuation of the TM and TE polarizations of the lower-order leaky modes.

The extinction ratio of such a graphene polarizer can be calculated by multiplying the difference in the attenuation constant by the propagation distance; that is, $(\alpha_{TM} - \alpha_{TE})L_G$. Theoretical results were compared with experimental observations (Fig. 4e), and revealed several important features. First, theoretical curves appear to be piecewise continuous, because each leaky mode has an identical cutoff wavelength (Fig. 4a). Second, the extinction ratio increases with increasing wavelength within each section. Finally, the experimental results measured at different wavelengths agree well with the performed simulations. Figure 4f shows the extinction ratio as a function of the length of the graphene film. The extinction ratio was found to be proportional to the propagation distance. Few-layer graphene has a slightly reduced extinction ratio with increasing thickness, as shown in the inset to Fig. 4f. This can be explained by the reduced damping of the TM mode resulting from the multiple conductivity of the few-layer graphene[30], whereas the attenuation of the TE mode remains largely unchanged. The difference between the extinction ratios of monolayer graphene and five-layer graphene is ~1 dB ($L_G = 3$ mm), which is quite close to the difference observed in the experiments (Fig. 2d).

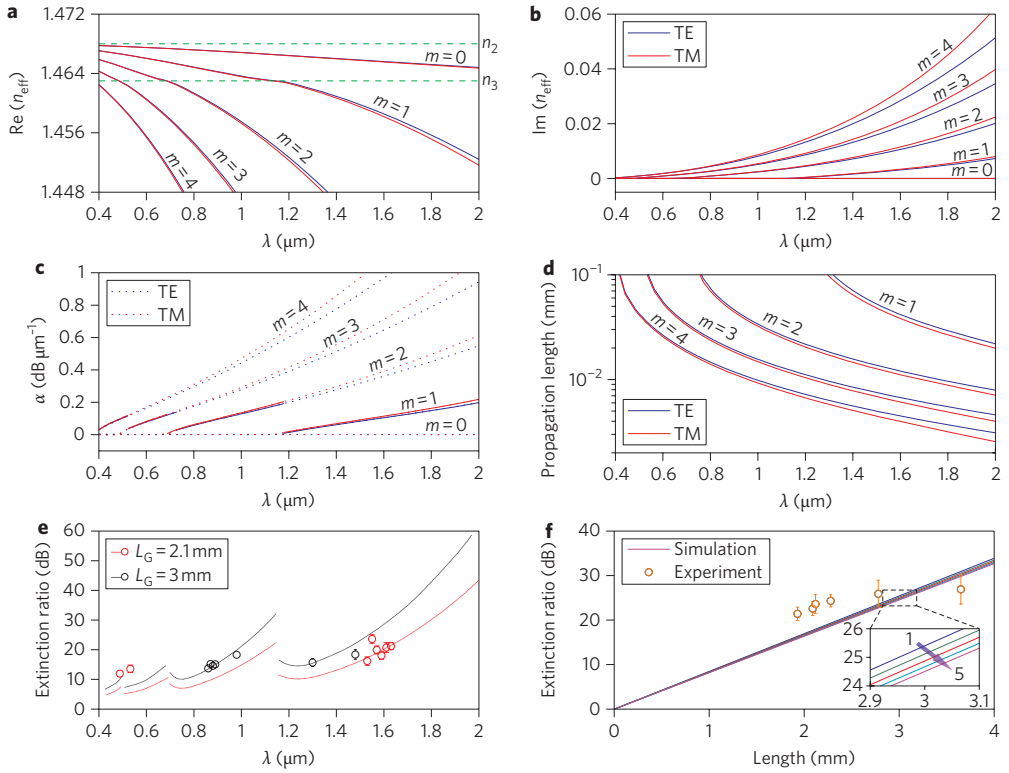

Figure 4 | Numerical calculation of electromagnetic modes in graphene. a, Real part of the effective index n_{eff} of the possible modes in a monolayer graphene–fibre hybrid waveguide. **b**, Imaginary part of n_{eff} for each mode. **c**, Attenuation of TM and TE polarizations of each mode. **d**, Propagation length of the TM and TE polarizations of each mode. **e**, Simulated broadband polarization effect in the visible–NIR range for monolayer graphene with different values of L_G. Solid dots, simulation results; open circles, experimental results. **f**, Simulated polarization extinction ratio (solid lines) as a function of L_G for a varying number of layers at 1,550 nm. Circles: experimental results for monolayer graphene.

Tuning the chemical potential allows the sign of complex conductivity to be varied sensitively at infrared frequencies. As explained by equations (3) and (4) (see Methods), the relative contribution of the intraband and interband conductivities varies with chemical potential and frequency, so tuning these affords some control over the propagation of the surface waves. Ideally, pristine graphene at $\mu = 0$ has no intraband Drude contribution, whereas the interband contribution extends from zero to the band edge and this supports the TE-mode surface wave. At $0 < |\mu| < \hbar\omega/2$, the interband contribution becomes larger at higher frequencies. If graphene is doped to a relatively high level ($|\mu| > \hbar\omega/2$), the interband conductivity becomes imaginary and the intraband contribution becomes dominant, thereby supporting the TM-mode surface wave[16,18]. The chemical potential of graphene can be modulated by electrical gating ($\mu \propto \mathrm{sgn}\, V_g\sqrt{V_g}$), or chemical doping, thus affording the possibility of making either a TE-pass or TM-pass graphene polarizer. Achieving such versatility in a metal-clad fibre polarizer is very difficult, as its mode selection is controlled by bulk properties and the thickness of the buffer layer.

In conclusion, we have studied the interaction of an electromagnetic field with graphene. A graphene TE-pass polarizer with an extinction ratio up to ~27 dB in the telecommunications band has been demonstrated. Numerical calculations reveal that the polarizing effect originates from the different attenuation of the TE and TM modes. The broadband polarizing effect of graphene from visible to NIR wavelengths provides an all-in-one solution for ultra-broadband light modulation, with the added advantages of simpler fabrication and lower cost than metal-clad polarizers. In addition, graphene affords the extra dimension of chemical tunability, which will allow the fabrication of environment-sensitive polarizers in the future.

Methods

Existence of the TE mode. Because graphene is a truly two-dimensional electronic system, the spectrum of the electromagnetic TM mode in a free-standing graphene sheet is governed by[19]

$$1 + \frac{2\pi j\sigma(\omega)\sqrt{q^2 - \omega^2/c^2}}{\omega} = 0 \tag{1}$$

and the TE mode has the form

$$1 - \frac{2\pi j\omega\sigma(\omega)}{c^2\sqrt{q^2 - \omega^2/c^2}} = 0 \tag{2}$$

Obviously, the TM mode exists only if the imaginary part of $\sigma(\omega)$ is positive and the TE mode if it is negative. The dynamic conductivity $\sigma(\omega)$ in graphene derived from the Kubo formula consists of both intraband and interband contributions[21,22]. Assuming $k_B T \ll |\mu|$, the intraband contribution can be simplified into the Drude-like form[18,28],

$$\sigma_{intra}(\omega) = \frac{je^2\mu}{\pi\hbar^2(\omega + j\tau^{-1})} \tag{3}$$

For $k_B T \ll |\mu|$ and $\hbar\omega$, the interband conductivity can be approximated as[21,22]

$$\sigma_{inter}(\omega) = \frac{je^2}{4\pi\hbar}\ln\left(\frac{2|\mu| - (\omega + j\tau^{-1})\hbar}{2|\mu| + (\omega + j\tau^{-1})\hbar}\right) \tag{4}$$

where $-e$ is the charge of an electron, $\hbar = h/2\pi$ is the reduced Planck's constant, ω is the radian frequency, k_B is Boltzmann's constant, T is temperature, μ is chemical potential, τ is the relaxation time, j is the imaginary unit and $e^{j\omega t}$ is the time variation. With $\sigma = \sigma' + j\sigma''$, it can be seen that $\sigma''_{intra} > 0$ if $\mu \neq 0$, so the TM mode is supported; $\sigma''_{inter} < 0$ if $\hbar\omega/2 > |\mu|$, the TE mode is supported.

Fabrication of the polarizer. Large-area monolayer and few-layer graphene films were grown by chemical vapour deposition on copper[30] and nickel[13], respectively. The layer thickness of the graphene was confirmed by optical contrast and Raman spectroscopy (Supplementary Fig. S1). A poly(methyl methacrylate) (PMMA) thin film with a thickness of ~100 nm was spin-coated onto the as-grown graphene film, followed by etching of the copper and nickel catalysts in $FeCl_3$ solution. PMMA-supported graphene films were then thoroughly rinsed in deionized water and transferred onto the planar region of the optical fibre by immersing the optical fibre beneath the water/graphene interface, followed by a gentle scooping of the graphene sheet onto the optical fibre. The sample was submerged in acetone to remove the PMMA. As-prepared samples were dried carefully under a gentle stream of N_2 gas before storage.

Optical measurements. The side of a single-mode optical fibre (SMF-28) was polished into the fibre core with a polished depth of ~1 μm (insertion loss, ~5 dB) to obtain a stronger interaction between the graphene waveguide and the electromagnetic field. Measurements were performed from the visible to the NIR range, with the experimental set-up differing according to the light sources used for each wavelength (see Supplementary Information for more details). For light sources with very weak polarization, the light was directly coupled into the graphene polarizer and another polarizer was placed after it to resolve the output power versus polarization angle (Supplementary Figs S4 and S5). For light sources with a certain polarization, the polarization state of the light coupled into the graphene polarizer was controlled by a half-wave plate and polarizer (Supplementary Figs S6 and S8). The output light (directly from the graphene polarizer) at varying polarization angles was monitored by a power/energy meter and an optical spectrum analyser. The experiments involved the coupling of light between free-space and optical fibres, with the fibres held as straight as possible to prevent additional birefringence.

Numerical model. Interaction between the electromagnetic wave and the graphene can be considered by solving Maxwell's equations and applying a microscopic quantum-dynamical model for a conductive surface. A semiclassical approach[16,19,28] was used and graphene was assumed to be a perturbation of a perfectly conducting planar waveguide. By matching the boundary conditions, the dispersion relation of the planar waveguide embedded with graphene could be achieved (see Fig. 3 and Supplementary Information for more details):

$$\mathrm{atan}(C_a) + \mathrm{atan}(C_b) + m\pi = \gamma_2 d \tag{5}$$

For TM modes,

$$C_a = \left(\frac{\gamma_1 \varepsilon_2}{\varepsilon_1 \gamma_2}\right)\left(1 + \frac{\sigma\gamma_1}{\omega\varepsilon_0\varepsilon_1}\right)^{-1}, \quad C_b = \frac{\gamma_3\varepsilon_2}{\varepsilon_3\gamma_2} \tag{6}$$

and for TE modes,

$$C_a = \left(\frac{\gamma_1 + \omega\mu_0\sigma}{\gamma_2}\right), \quad C_b = \frac{\gamma_3}{\gamma_2} \tag{7}$$

where m is the order of the mode, ε_i is the relative permittivity of region i, $\gamma_1 = \sqrt{\beta^2 - \varepsilon_1 k_0^2}$, $\gamma_2 = \sqrt{\varepsilon_2 k_0^2 - \beta^2}$ and $\gamma_3 = \sqrt{\beta^2 - \varepsilon_3 k_0^2}$, $k_0 = \omega/c$ is the free-space wavenumber, c is the speed of light in vacuum, and d is the distance between interfaces a and b (Fig. 3c).

Received 6 October 2010; accepted 22 April 2011; published online 29 May 2011

References

1. Goldstein, D. *Polarized Light* 2nd edn (Marcel Dekker, 2003).
2. Bergh, R., Lefevre, H. & Shaw, H. Single-mode fiber-optic polarizer. *Opt. Lett.* **5,** 479–481 (1980).
3. Feth, J. & Chang, C. Metal-clad fiber-optic cutoff polarizer. *Opt. Lett.* **11,** 386–388 (1986).
4. Dyott, R. B., Bello, J. & Handerek, V. A. Indium-coated D-shaped-fiber polarizer. *Opt. Lett.* **12,** 287–289 (1987).
5. Andreev, A. T., Kozlov, V., Kuznetsov, A. & Maksimov, A. Single-mode fiber polarizers for the spectral range 0.6–1.6 μm. *Quantum Electron.* **23,** 617–619 (1993).
6. Tseng, S. M., Hsu, K. Y., Wei, H. S. & Chen, K. F. Analysis and experiment of thin metal-clad fiber polarizer with index overlay. *IEEE Photon. Technol. Lett.* **9,** 628–630 (1997).
7. Li, G. Y. & Xu, A. S. Analysis of the TE-pass or TM-pass metal-clad polarizer with a resonant buffer layer. *J. Lightwave Technol.* **26,** 1234–1241 (2008).
8. Neto, A. H. C., Guinea, F., Peres, N. M. R., Novoselov, K. S. & Geim, A. K. The electronic properties of graphene. *Rev. Mod. Phys.* **81,** 109–162 (2009).
9. Bonaccorso, F., Sun, Z., Hasan, T. & Ferrari, A. C. Graphene photonics and optoelectronics. *Nature Photon.* **4,** 611–622 (2010).
10. Loh, K. P., Bao, Q., Eda, G. & Chhowalla, M. Graphene oxide as a chemically tunable platform for optical applications. *Nature Chem.* **2,** 1015–1024 (2010).
11. Nair, R. R. *et al.* Fine structure constant defines visual transparency of graphene. *Science* **320,** 1308 (2008).
12. Mueller, T., Xia, F. N. A. & Avouris, P. Graphene photodetectors for high-speed optical communications. *Nature Photon.* **4,** 297–301 (2010).
13. Bao, Q. *et al.* Atomic-layer graphene as a saturable absorber for ultrafast pulsed lasers. *Adv. Funct. Mater.* **19,** 3077–3083 (2009).
14. Sun, Z. *et al.* Graphene mode-locked ultrafast laser. *ACS Nano* **4,** 803–810 (2010).
15. Horing, N. J. M. Coupling of graphene and surface plasmons. *Phys. Rev. B* **80,** 193401 (2009).
16. Hanson, G. W. Dyadic Green's functions and guided surface waves for a surface conductivity model of graphene. *J. Appl. Phys.* **103,** 064302 (2008).
17. Mishchenko, E. *et al.* Guided plasmons in graphene pn junctions. *Phys. Rev. Lett.* **104,** 156806 (2010).
18. Jablan, M., Buljan, H. & Soljacic, M. Plasmonics in graphene at infrared frequencies. *Phys. Rev. B* **80,** 245435 (2009).
19. Mikhailov, S. & Ziegler, K. New electromagnetic mode in graphene. *Phys. Rev. Lett.* **99,** 016803 (2007).
20. Stern, F. Polarizability of a two-dimensional electron gas. *Phys. Rev. Lett.* **18,** 546–548 (1967).
21. Peres, N. M. R., Guinea, F. & Castro Neto, A. H. Electronic properties of disordered two-dimensional carbon. *Phys. Rev. B* **73,** 125411 (2006).
22. Gusynin, V. P., Sharapov, S. G. & Carbotte, J. P. Unusual microwave response of Dirac quasiparticles in graphene. *Phys. Rev. Lett.* **96,** 256802 (2006).
23. Maier, S. *Plasmonics: Fundamentals and Applications* 1st edn (Springer Verlag, 2007).
24. Johnstone, W., Stewart, G., Hart, T. & Culshaw, B. Surface-plasmon polaritons in thin metal-films and their role in fiber optic polarizing devices. *J. Lightwave Technol.* **8,** 538–544 (1990).
25. Ohke, S., Umeda, T. & Cho, Y. TM-mode selective filter using leaky waveguide structure. *Electron. Comm. Jap. II: Electron.* **85,** 9–15 (2002).
26. Rollke, K. H. & Sohler, W. Metal-clad waveguide as cutoff polarizer for integrated-optics. *IEEE J. Quantum Electron.* **13,** 141–145 (1977).
27. Berini, P. Plasmon-polariton modes guided by a metal film of finite width. *Opt. Lett.* **24,** 1011–1013 (1999).
28. Hanson, G. W. Quasi-transverse electromagnetic modes supported by a graphene parallel-plate waveguide. *J. Appl. Phys.* **104,** 084314 (2008).
29. Okamoto, K. *Fundamentals of Optical Waveguides* (Academic Press, 2006).
30. Bae, S. *et al.* Roll-to-roll production of 30-inch graphene films for transparent electrodes. *Nature Nanotech.* **5,** 574–578 (2010).

Acknowledgements

This work was supported by an NRF-CRP grant ('Graphene Related Materials and Devices', R-143-000-360-281). The authors thank R.J. Knize (United States Air Force Academy) for helpful discussions, B. Yan, T. Yu and Z.X. Shen (SPMS, NTU) for assistance with measurements at visible wavelengths, and X. Wu, L.M. Zhao and B. Lin (EEE, NTU) for assistance with measurements at near-infrared wavelengths. H.Z. acknowledges financial support from the Belgian Science Policy Office (BELSPO) Interuniversity Attraction Pole (IAP) programme (grant no. IAP-6/10) and experiment facility support from OPERA-photonique (Université libre de Bruxelles). The authors thank P. Kockaert, P. Emplit and M. Haelterman (Université libre de Bruxelles) for discussion and critical reading of this manuscript.

Author contributions

K.P.L. supervised the project. K.P.L. and Q.B. planned the project. Q.B. and H.Z. conceived the original concept and performed most of the experiments. B.W. and Q.B. contributed to the numerical calculations. Z.N. contributed to measurements in the visible range. H.Z. and D.Y.T. contributed to the experiments in the NIR range. C.H.Y.X.L. and Y.W. contributed to graphene synthesis. K.P.L. and Q.B. analysed the data and co-wrote the paper. All authors discussed the results and commented on the manuscript.

Additional information

The authors declare no competing financial interests. Supplementary information accompanies this paper at www.nature.com/naturephotonics. Reprints and permission information is available online at http://www.nature.com/reprints/. Correspondence and requests for materials should be addressed to K.P.L.